Green Light Promoted Iridium(III)/Copper(I)-Catalyzed Addition of Alkynes to Aziridinoquinoxalines Through the Intermediacy of Azomethine Ylides

Oleksii Zhelavskyi,[a] Seren Parikh,[a] Richard J. Staples,[b] Paul M. Zimmerman,*[a] and Pavel Nagorny*[a]

Department of Medicinal Chemistry, University of Michigan, Ann Arbor, Michigan 48109, United States[a]
Department of Chemistry and Chemical Biology, Michigan State University, East Lansing, MI 48824[d]

Aziridines, quinoxalines, alkyne addition, photochemical, asymmetric catalysis

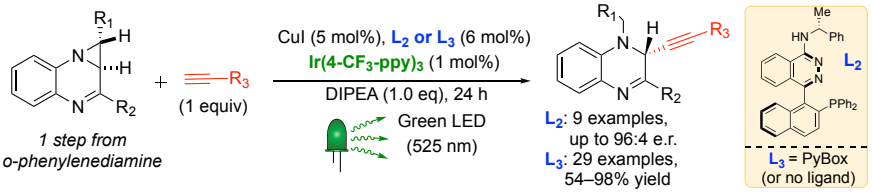

ABSTRACT: This manuscript describes the development of alkyne addition to the aziridine moiety of aziridinoquinoxalines using dual Ir(III)/Cu(I) catalytic system under green LED photolysis (λ_{max} = 525 nm). This mild method features high levels of chemo- and regioselectivity and was used to generate 29 highly functionalized substituted dihydroquinoxalines in 44-98% yield. This transformation was also carried asymmetrically using *(S,R)-N*-PINAP as the chiral ligand to provide 9 chiral addition products in 96:4 to 86:14 e.r. The experimental and quantum chemical explorations of this reaction suggest a mechanism that involves Ir(III)-catalyzed triplet energy transfer mechanism followed by a ring-opening reaction ultimately leading to the formation of azomethine ylide intermediates. These azomethine intermediates undergo sequential protonation/copper(I) acetelide addition to provide the products.

Introduction

Due to their high occurrence in nature and unique chemical properties, nitrogen-containing heterocycles are of great importance to various areas of drug discovery, AgroSciences, and material science.[1] Nitrogen-containing heterocycles are present in essential biomolecules such as DNA, RNA and proteins. Recent analysis of the US FDA approved pharmaceuticals highlights the importance of the nitrogen containing heterocyclic molecules as 59% of unique drugs contained at least one nitrogen heterocycle, and the average number of nitrogen atoms per drug was found to be 2.3 N/drug.[1b] The continuously increasing interest to nitrogen-containing heterocyclic compounds has fueled the development of many creative synthetic methodologies to access various nitrogen-containing scaffolds, particularly in their enantiopure forms.[2] These studies have been enabled by the recent advances in asymmetric catalysis, photocatalysis, transition metal catalysis and organocatalysis as well as development of new mechanistic concepts for harnessing the reactivity of highly reactive intermediates.[3] Among various heterocycles, significant efforts have been focused in achieving synthesis of substituted tetrahydroquinoxalines (Figure 1). These heterocyclic motifs are present in a variety of bioactive compounds such as molecules **1–3** (Figure 1A).[4] The standard approaches to chiral tetrahydroquinoxalines involve hydrogenation or transfer hydrogenation of quinoxalines, which poses limitations to the types of products that could be accessed through these reductive methods.[5] At the same time, recent advances in catalysis enabled asymmetric synthesis of complex tetrahydroquinoxalines that are not easily accessible through dearomative reduction of quinoxalines (Figures 1B-D).[6]

The Nagorny group has long-standing interests in developing new catalytic methods for the synthesis of chiral heterocyclic molecules of medicinal chemistry value.[7] Our recent studies highlighted the use of both Ir(III)-based catalysts[7c] and Chiral Phosphoric Acids (CPAs)[7b,e] for the synthesis of chiral nitrogen-based heterocycles. Among various chiral heterocyclic systems that we have explored as substrates for the CPA-catalyzed transfer hydrogenation are aziridinoquinoxalines **6** (Figure 2B).[7e] These unusual heterocycles could be generated in one step from *o*-phenylenediamines (**4**) by their condensation with a,b-dibromoketones (**5**).[7e,8] Previously, we demonstrated that aziridinoquinoxalines (**6a**) may undergo chemoselective C=N addition upon exposure to nucleophiles (*cf.* Figure 2B and SI-II-5) while the aziridine moiety stays intact. However, this manuscript summarizes our studies that demonstrates that this reactivity could be completely switched under the photochemical conditions and that the aziridine moiety could be selectively reacted with copper(I) acetylides[9-11] in the presence of the imine (C=N) group to provide previously inaccessible dihydroquinoxalines. This reaction between alkynes and aziridinoquinoxalines (**6**) is promoted under mild photochemical conditions using green LED light (λ_{max}=525 nm) and is co-catalyzed by Ir(III) and Cu(I) catalysts (Figure 1E). In addition, the described studies demonstrate that this transformation could be carried asymmetrically using PINAP as the ligand (**L2**).[10d,12]

The presence of two electrophilic sites makes aziridinoquinoxalines to be versatile precursors for the synthesis of highly functionalized quinoxalines. While these species have not been extensively explored, prior work suggests that both the

C=N imine moiety and the aziridine ring may participate in reactions (Figure 2A).[8] The prior studies exploring the reactivity

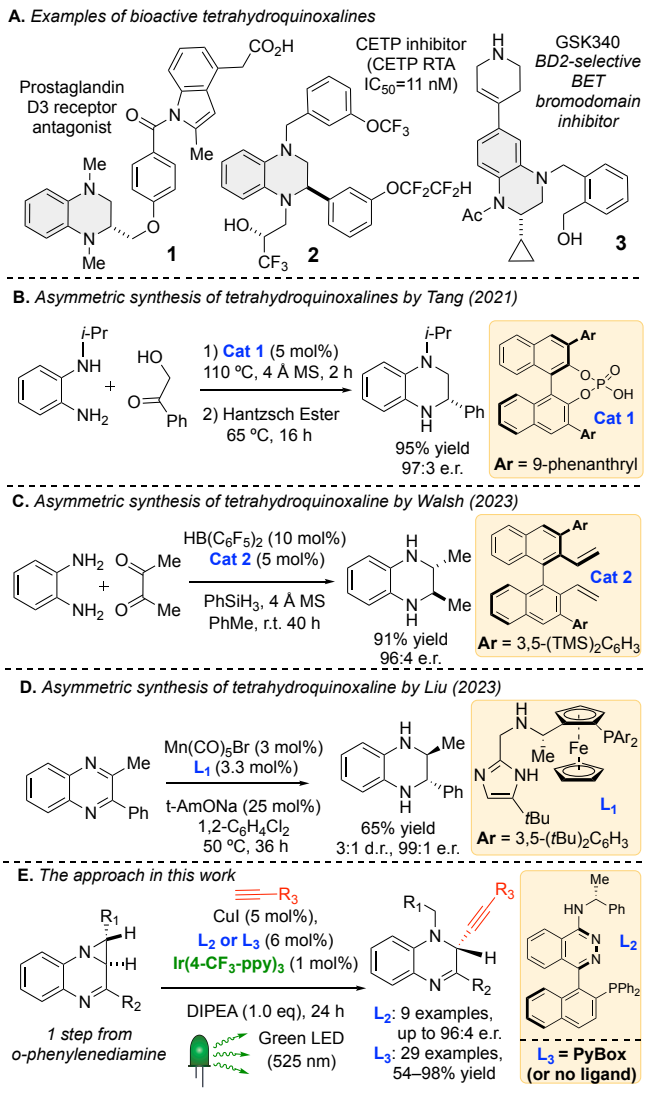

Figure 1. Recent approaches chiral tetrahydroquinoxalines

of **6a** and related compounds suggest that these compounds may undergo thermal 4π-electrocylic ring-opening reaction to provide azomethine ylides that could be intercepted in various [3+2] cycloaddition reactions with alkenes, alkynes, aldehydes and diazo dicarboxylates.[8a] It is noteworthy that 4π-electrocylic ring-opening of **6a** requires significantly lower temperatures than the corresponding reaction of an inactivated aziridine ring (110-150 °C vs. 200-250 °C).[13] At the same time, our studies demonstrate that under normal conditions aziridinoquinoxalines such as **6a** may undergo polar reactions with nucleophiles at the C=N group, rather than aziridine, moiety. Thus, when **6a**/**6d** was exposed to copper(I)-catalyzed allylation reaction with allyl silane, C=N addition products **7a**/**7d** were obtained in excellent yield (*cf.* SI-II-5). Similarly, when exposed to standard transfer hydrogenations with Hatzsch ester and (*R*)-TRIP catalyst, **(±)-6a** underwent chemo- and enantioselective hydride addition to the C=N group to provide chiral diastereomeric products **8a** and **9a** (Figure 2B).[7e]

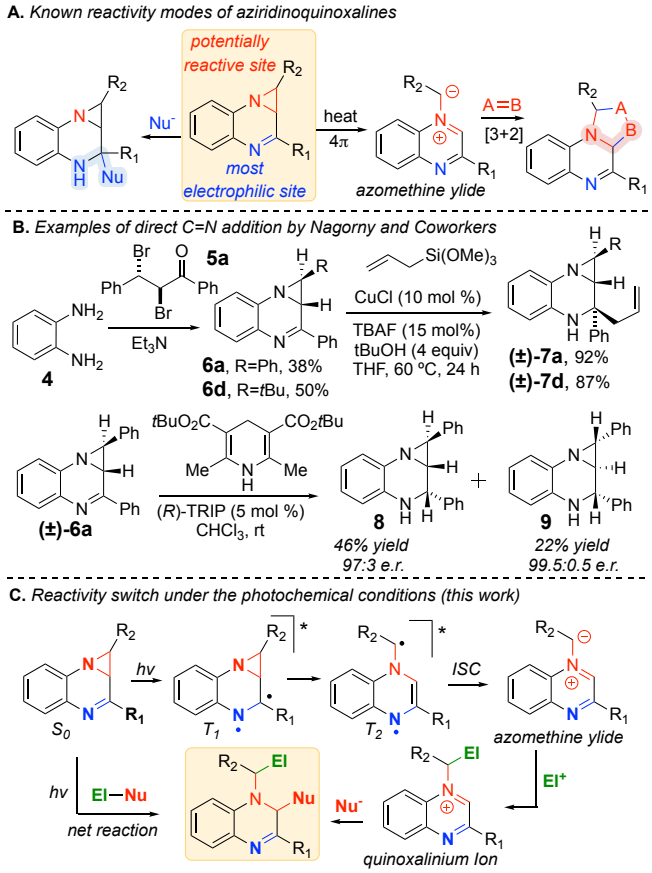

Figure 2. Reactivity of aziridinoquinoxalines and proposed photoactivation of the aziridine moiety

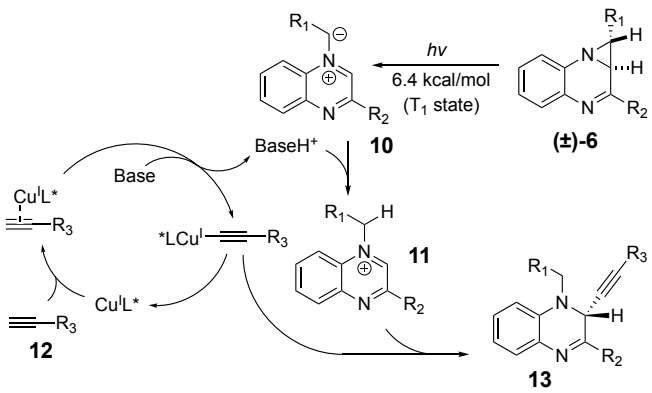

Scheme 1. Mechanistic cycle for the Cu(I)-catalysed photochemical addition of acetylenes 12 to aziridinoquinoxalines 6

One of the interesting physicochemical properties of aziridinoquinoxalines such as **6a** is photochromism.[14] Thus, it was noted that **6a** may undergo reversible change in color from yellow to red upon exposure to sun light.[8c] While this phenomenon was attributed to the reversible formation of strongly colored azomethine ylide in solid state, photochemical properties, and reactivity of **6** and related aziridinoquinoxalines under photochemical conditions have not been explored in details.[15]

Based on the prior work[16] and our computational and experimental results (*vide infra*), we surmised that photoexcitation of **6** in its ground state (S_0) may produce its triplet state T_1, which may undergo an aziridine ring fragmentation to intermediate T_2 followed by a low-barrier Intersystem Crossing (ISC) step leading to the azomethine ylide formation (Figure 2C). The ylide, generated under mild conditions, may undergo polar reactions with electrophiles and nucleophiles to provide functionalized tetrahydroquinoxalines that are otherwise not accessible through other methods.[17]

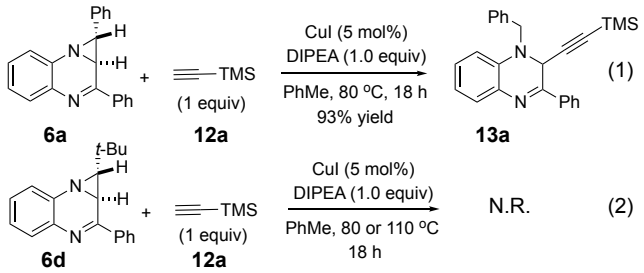

Results and Discussion

Based on the mechanistic considerations presented in Figure 2, we surmised that azomethine ylides derived from aziridinoquinoxalines (**6**) might be intercepted with copper(I) acetylides[10j,18] through the catalytic cycle summarized in Scheme 1. The photoactivation of aziridinoquinoxalines is expected to provide azomethine ylide **10**, which is expected to be protonated with ammonium salts generated during the formation of copper(I) acetylide. The resultant quinoxalinium ion **11** would be trapped with copper(I) acetylide to produce the desired product **13** and regenerate Cu(I) salt, which would reengage in the catalytic cycle. Our studies commenced with exploring the proposed in Scheme 1 catalytic cycle under the thermal activation conditions that was previously observed to convert substrate **6a** into the corresponding ylides (Eq. 1 and 2). Initial reaction optimization involved selecting the optimal reaction temperature, stoichiometry, and catalyst loading (cf. Table SI-1). The efficient formation of product **13a** (93% yield) was observed under the optimized conditions after heating the substrate for 18 h at 80 °C using 5 mol% of Cu(I) iodide as the catalyst and DIPEA as the base. Further elevation of the temperature led to shorter reaction times; however, the formation of side-product and decomposition impurities was observed lowering the product yield. Unfortunately, our attempts to extend this method to other substrates such as the *t*-butyl-substituted aziridinoquinoxalines **6d**, did not lead to the formation of the desired product, even at 110 ºC. This, coupled with only moderate enantioselectivities observed for **13a** with chiral ligands under thermal activation (*cf.* Tables SI-2 and SI-3) prompted us to pursue the photochemical activation of **6** next.

The possibility of photochemical pathway was evaluated by DFT computations (B3LYP/6-31+G** and SMD(Toluene)/wB97x-D3/cc-pVTZ, *cf.* SI-IV-1) where the Growing String Method (GSM)[19] was used to compute the ring-opening energy barriers (Table 1) in both the ground singlet state (S_0) as well as the excited triplet state (T_1). For aziridine **6a**, the activation energy was found to be $\Delta G^{\ddagger}$ = 32.5 kcal/mol for ring-opening in the S_0-state, which is in good

Table 1. Computed Energy Barriers for Photoinduced Ring-Opening of aziridinoquinoxalines 6a-6d and 8a.[a]

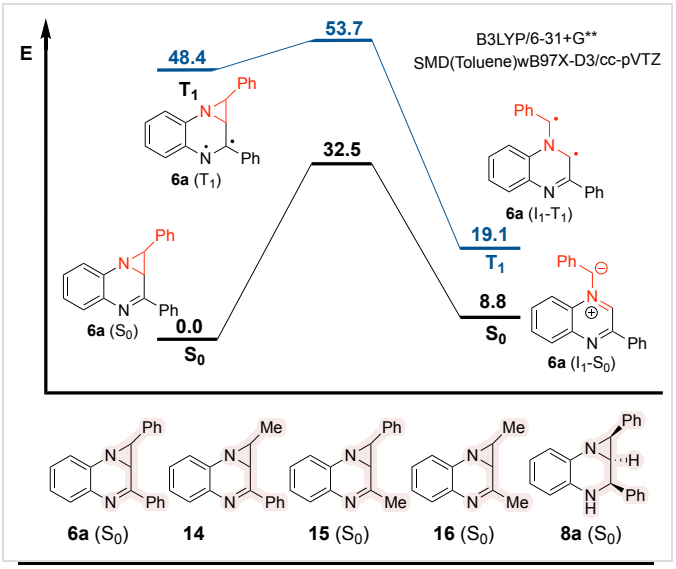

E (kcal/mol)	6a	14	15	16	8a
$\Delta G^{\ddagger}(S_0)$	32.5	40.9	34.5	42.8	44.0
I_1-S_0	8.8	6.2	8.3	6.4	29.2
T_1	48.4	48.3	57.3	57.5	82.9
$\Delta G^{\ddagger}(T_1)$[b]	4.7 (53.7)	10.1 (58.4)	1.0 (63.6)	6.1 (63.6)	4.4 (87.3)
I_1-T_1	19.1	28.2	19.1	29.4	46.6

[a] The provided energies were computed using DFT (B3LYP/6-31+G** and SMD(Toluene)/wB97x/cc-pVTZ) and Growing String Method (GSM) (*cf.* SI-iV-1 for additional details). [b] The values in parenthesis represent the relative values of the computed transition states to the ground S_0 state of corresponding aziridinoquinoxalines.

agreement with the observed reactivity under the thermal activation conditions (Eq. 1). However, the computed energy barrier for ring-opening in T_1 state is only 4.7 kcal/mol, and the formation of ylide **6a** (I_1-T_1) in triplet state is also more thermodynamically favored by 29.3 kcal/mo. The triplet state for compound **1a** is photochemically accessible at 48.4 kcal/mol above S_0. Results from these simulations in Table 1 also explain the low reactivity of alkyl-substituted aziridines such as **6b** in thermally activated ring-opening (Eq. 2). The predicted thermal activation energy barrier from the S_0 state is much higher for the alkyl-substituted substrates such as **14** and **16** (about 40.9 and 42.8 kcal/mol, correspondingly); however, the photochemically induced ring-opening of alkyl aziridines is more feasible from T_1 state due to significantly lower barriers (10.1 and 6.1 kcal/mol, correspondingly). It is noteworthy that changing the C_2-phenyl substituent in the aziridinoquinoxaline ring to a methyl group (models **15** and **16**) results in significant increase of

the T_1-state energies by ~9 kcal/mol due to the weaker radical stabilization. Finally, replacing the imine (C=N) chromophore with the CH–NH moiety present in **8a** renders the photochemical process infeasible due to the highly unstable triplet state **8a**-T_1 (82.9 kcal/mol).

Table 2. Optimization of photochemical addition of alkyne 12a to aziridinoquinoxalines 6a.[a]

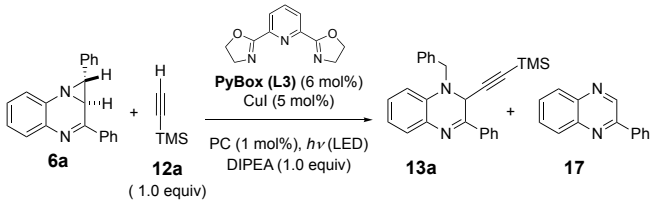

entry	λ (nm)	PC	Solvent	time (h)	Conv. (%)[b]	**13a:17**
1	440	–	PhMe	6	>95	0:100
2	440	–	THF	6	>95	0:100
3	440	Ir(dF-ppy)$_3$	THF	6	>95	0:100
4	440	Ir(4-CF$_3$-ppy)$_3$	THF	6	>95	22:78
5	525	–	THF	24	<5	–
6	525	Ir(4-CF$_3$-ppy)$_3$	THF	24	68	64:36
7	525	–	PhMe	24	26	84:16
8	525	Ir(4-CF$_3$-ppy)$_3$	PhMe	24	>95	93:7
9	525	Ir(ppy)$_3$	PhMe	24	>95	84:16
10	525	Ir(ppy)$_2$(4,4'-dtbbpy)	PhMe	24	11	65:35
11	525	[Ir(dF(CF$_3$)ppy)$_2$ (dtbbpy)]PF$_6$	PhMe	24	21	–
12	525	Eosin Y	PhMe	24	0	–

[a] The reaction was performed on 0.1 mmol scale using 0.05 M solution in the corresponding solvent as described in SI-II-2.

Based on the modeling results of Table 1, our subsequent studies focused on exploring the direct excitation of aziridinoquinoxaline **6a** with Blue LED (λ_{max}=440 nm) (Table 2). Achiral PyBox ligand was used to solubilize copper(I) iodide. After 6 h, complete consumption of **6a** was observed in both toluene and THF leading to the ylide decomposition product 2-phenylquinoxaline **17** (entries 1 and 2). Introducing Ir(III) photocatalysts (entries 3 and 4) didn't significantly improve the reaction outcome, and only with Ir(4-CF_3ppy) the formation of minor amounts of **13a** was observed along with **17** in 22:78 ratio.[20]

To understand the reasons behind the nonproductive substrate **6a** decomposition and to identify better conditions for the photochemical activation, time-dependent DFT calculations (TD-DFT, SMD(Toluene)/wB97x-D3/cc-pVTZ) were performed to characterize excited states of the compound **6** and their ylides (Scheme 2A and SI-IV-5). For compound **6a**, the first excited state S_1 was found to have a vertical excitation energy of 92.1 kcal/mol (313 nm) and oscillator strength 0.35. Geometry optimization gives the lowest point of the S_1 PES at 79.7 kcal/mol (359 nm). This implies that direct excitation of **6a** is possible with the Kessil Blue LED source (Figure SI-1). Computational results are also in good agreement with the experimental UV-VIS spectra of **6a** (Figure SI-3) and fluorescence spectroscopy measurements that indicated emission at 337 nm and absorption at 305 nm for the S_0-S_1 transition (Scheme 2B, Figure SI-10).

Singlet-excited compound **6a** (S_1) may undergo an intersystem crossing to its triplet state **6a** (T_1), which has an energy of 50.4 kcal/mol (567 nm). The T_1 state is close to detected fluorescence emission peak at 515 nm (see Scheme 2C, Figure SI-11). Therefore, the T_1 state could be responsible for photoactivation of **6a** under the tested conditions. In particular, aziridine ring opening transforms the initial triplet geometry of **6a** (T_1) (50.4 kcal/mol) to a much lower energy structure (I_1-T_1) (12.1 kcal/mol), as shown in Scheme 2A. I_1-T_1 then can nonradiatively relax to the ring opened, ground I_1-S_0 state. From that point, TD-DFT analysis of the ylide intermediate **6a** (I_1-S_0) indicated an S_0-S_1 excitation at 73.8 kcal/mol (441 nm) with a substantial oscillator strength of 0.92.[21] The ylide's S_0-S_1 energy gap is well within reach of the Blue LED, and its high oscillator strength makes the ylide intermediate **6a** (I_1-S_0) photoactive. As a result, low yields of the desired product **13a** can be explained by an undesired pathway that involves the excitation of intermediate **6a** (I_1-S_0) by Blue LED at 440 nm, which leads to its decomposition.

In general, all other model substrates **14-16** (*cf.* SI-Scheme SI-10) produce photoactive ylides with accessible S_0-S_1 transitions. The photoexcited states are reachable due to the greater extent of conjugation in the open forms of aziridines. Methyl substituents at the C_1-position of aziridines **14** and **16** do not have any impact on the energies of the triplet states T_1, while making the corresponding ylides **14** (I_1-S_0) and **16** (I_1-S_0) less stable and photoactive due to the absence of the additional aromatic conjugation such as the one that is present in compound **6a**. It is worth noting that the ylide derived from the C_2-phenyl containing substrate **14** absorbs shorter wavelength due to the alkyl substituent in the aziridine ring and should be more stable to decomposition under the photochemical conditions. In contrast, switching the phenyl substituent at the C_2-position of the quinoxalinium core to the methyl group (substrates **15** and **16**) destabilizes both excited singlet (S_1) and triplet (T_1) states of **15** and **16**. In summary, avoiding excitation of the ylide intermediates under the reaction conditions should eliminate decomposition pathways. This can be achieved by switching to light sources with a longer wavelength (>475 nm) and establishing energy triplet transfer (EnT) through a photocatalyst that selectively promotes the S_0-T_1 transitions.

Guided by the considerations above, we implemented a less energetic light source by switching to Green LED (525 nm, emission spectrum Figures SI-2) to avoid the excitation of the

Scheme 2. Computational and spectroscopic studies to optimize the photochemical ring-opening of 6a and substrate scope exploration studies.

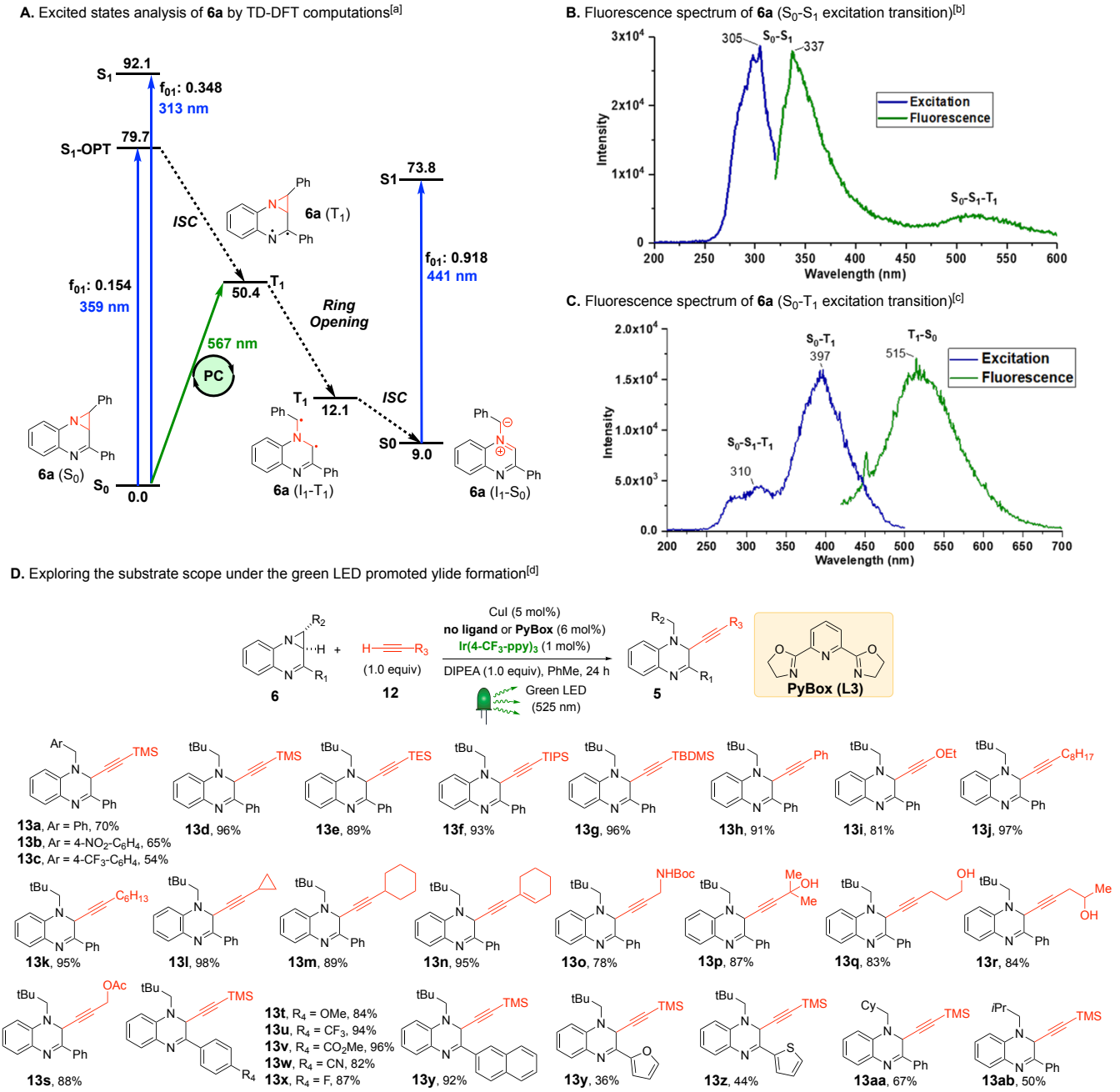

[a] Time-dependent DFT calculations (TD-DFT) were performed using SMD(Toluene)/wB97x-D3/cc-pVTZ (*cf.* SI-IV-5 for additional details). [b] The fluorescence excitation spectroscopy (green – fluorescence spectrum excited at 305 nm, blue – absorption spectrum for fluorescence detected at 337 nm) of 50 μM solution of **6a** in THF; [c] The fluorescence excitation spectroscopy (green – fluorescence spectrum excited at 397 nm, blue – absorption spectrum for fluorescence detected at 515 nm) of 50 μM solution of **6a** in THF; [d] The reactions were carried on 0.1 mmol scale described in SI-II-2. Reactions leading to **13d–13z** were performed without **PyBox** Ligand, and the formation of substrates **13a-13c, 13aa-13ab** were carried with 6 mol% of **PyBox**.

ylide intermediates (*cf.* Table 2, entries 5-12). As expected, we do not observe any reaction of **6a** in THF when exposed to Green LED alone (entry 5) as the light with l_{max} = 525 nm cannot effectively excite aziridinoquinoxalines such as **6a**. Introducing Ir(III) photocatalyst Ir(4-CF_3-ppy)$_3$ allowed us to achieve higher conversion in THF (Entry 6) with much better 64:36 product **13a** to **17** ratio. Reaction in toluene without photocatalyst was also not effective albeit provided some observable product (entry 7). However, the reaction progression was significantly improved when Ir(4-CF_3-ppy)$_3$ was used as the photocatalyst, and the reaction reached full conversion in 24 hours resulting in almost pure product **13a** (Entry 8). Further

photocatalyst screening did not lead to improvement (entries 9-12) although the observed results were in good agreement with the proposed EnT mechanism. Ir(ppy)$_3$ both matches the triplet state energy and has a relatively long T_1 lifetime, and this catalyst was found to have a similar catalytic activity to Ir(4-CF_3-ppy)$_3$ (entry 9). Ir(ppy)$_2$(4,4'-dtbbpy) photocatalyst in entry 10 has too low triplet energy (49.2 kcal/mol) while [Ir(dF(CF_3)ppy)$_2$(dtbbpy)]PF_6 catalyst in entry 11 is probably mismatched with the triplet gap of compound **6a**. Eosin Y is similar to Ir(4-CF_3ppy)$_3$ in terms of its triplet state energy,[20] but it has shorter excited state lifetime to promote EnT mechanism. Using organic dye, Eosin Y, (entry 12) with the absorption at 520 nm that matches well the employed light source with λ_{max}=525 nm neither lead to the formation of product nor to decomposition. This may be attributed to the low triplet state energy of Eosin Y or to low solubility of Eosin Y in toluene.

Table 3. Optimization of enantioselective 6a.[a]

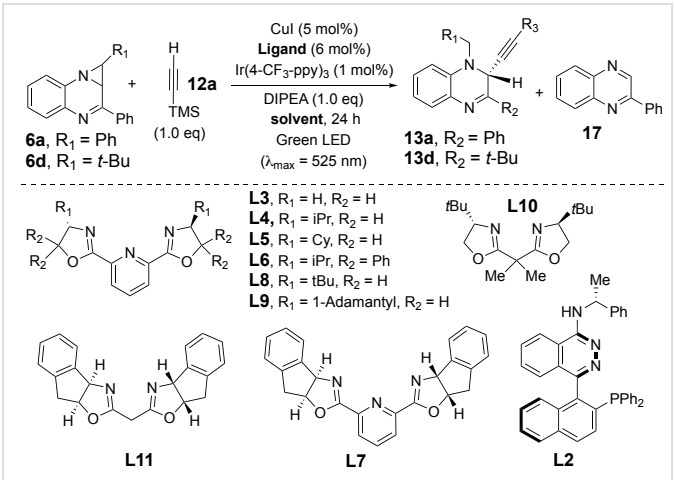

entry	solvent	ligand	substrate	conversion/yield (%)[b]	13:17	e.r.
1	PhMe	**L4**	**6a**	>95	93:7	72:28
2	PhMe	**L5**	**6a**	>95	89:11	55:45
3	PhMe	**L6**	**6a**	>95	90:10	63:37
4	PhMe	**L7**	**6a**	>95	67:33	57:43
5	PhMe	**L8**	**6a**	>95	83:17	82:18
6	PhMe	**L9**	**6a**	>95	87:13	82:18
7[c]	PhMe	**L9**	**6a**	>95	78:22	86:14
8[c]	PhMe	**L8**	**6a**	>95/67	81:19	87:13
9	PhMe	**L2**	**6a**	>95/28	55:45	93:7
10	THF	**L2**	**6a**	>95/25	49:51	95:5
11	THF	**L2**	**6d**	>95/81	98:2	93:7

[a] The reactions were performed on 0.1 mmol scale using 0.05 M solution in specified solvent as described in SI-II-2. [b] The conversion was determined by ^{1}H NMR analysis of the crude reaction mixture. [c] These reactions were performed with 2.5 mol% of copper(I) iodide and 5 mol% of **L9** or **L8**.

With the optimized protocol in hand, the substrate scope evaluation was performed next by exploring the variations in alkynes **12** and aziridinoquinoxalines **6** (Scheme 2D). As expected, the introduction of the electronwithdrawing substituents to the phenyl ring attached to the aziridine moiety had a minor effect on the reaction yield, and substrates **13b** and **13c** were obtained in 65% and 54%, correspondingly. Due to much lower energy barrier for ring-opening in T_1 triplet state, *t*Bu-substituted aziridinoquinoxaline **6d**, previously unreactive under the thermal activation conditions, was successfully converted to product **13d** in 96% yield using the green LED/Ir(III) activation protocol.

Scheme 3. Enantioselective alkyne addition with ligand L2

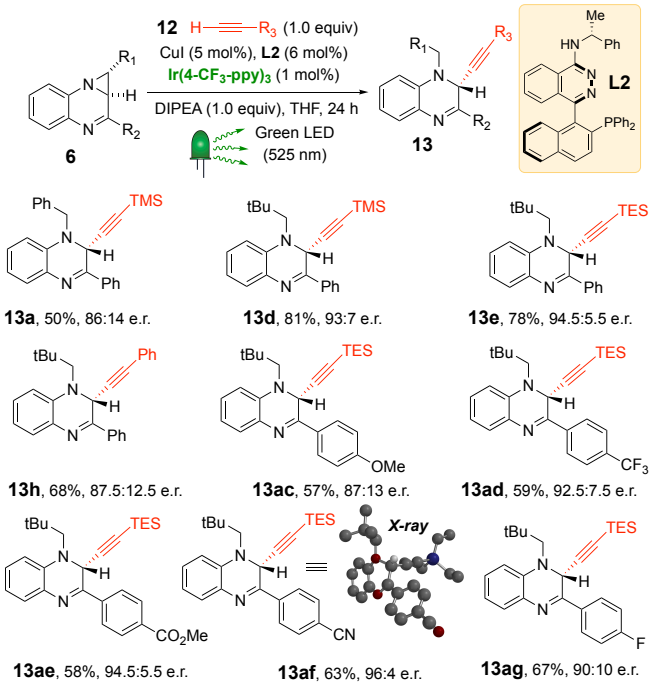

[a] The reactions were performed on 0.1 mmol scale using 0.05 M solution in THF as described in SI-II-2.

In general, compound **6d** was significantly more stable under the photochemical conditions than **6a** (that provided product **13a** in only 70% yield) and other aryl-substituted aziridines such as **13b** and **13c**. Reaction proceeds with excellent yields (>90%) with a wide range of alkynes including various silyl-protected alkynes **12e-12g**, phenylacetylene **12h**, ethoxyacetylene **12i**, alkyl substituted acetylene **12j** and **12k**, and cyclohexyl-substituted **13m**. Alkynes with photolabile groups such as cyclohexene group (**13n**) and cyclopropyl group (**13l**) that can form radicals under photochemical excitation are well tolerated under the green LED radiation with λ_{max}=525 nm. Presence of the potentially nucleophilic groups such as amines and

Scheme 4. Experimental and computational exploration of the reaction mechanism.

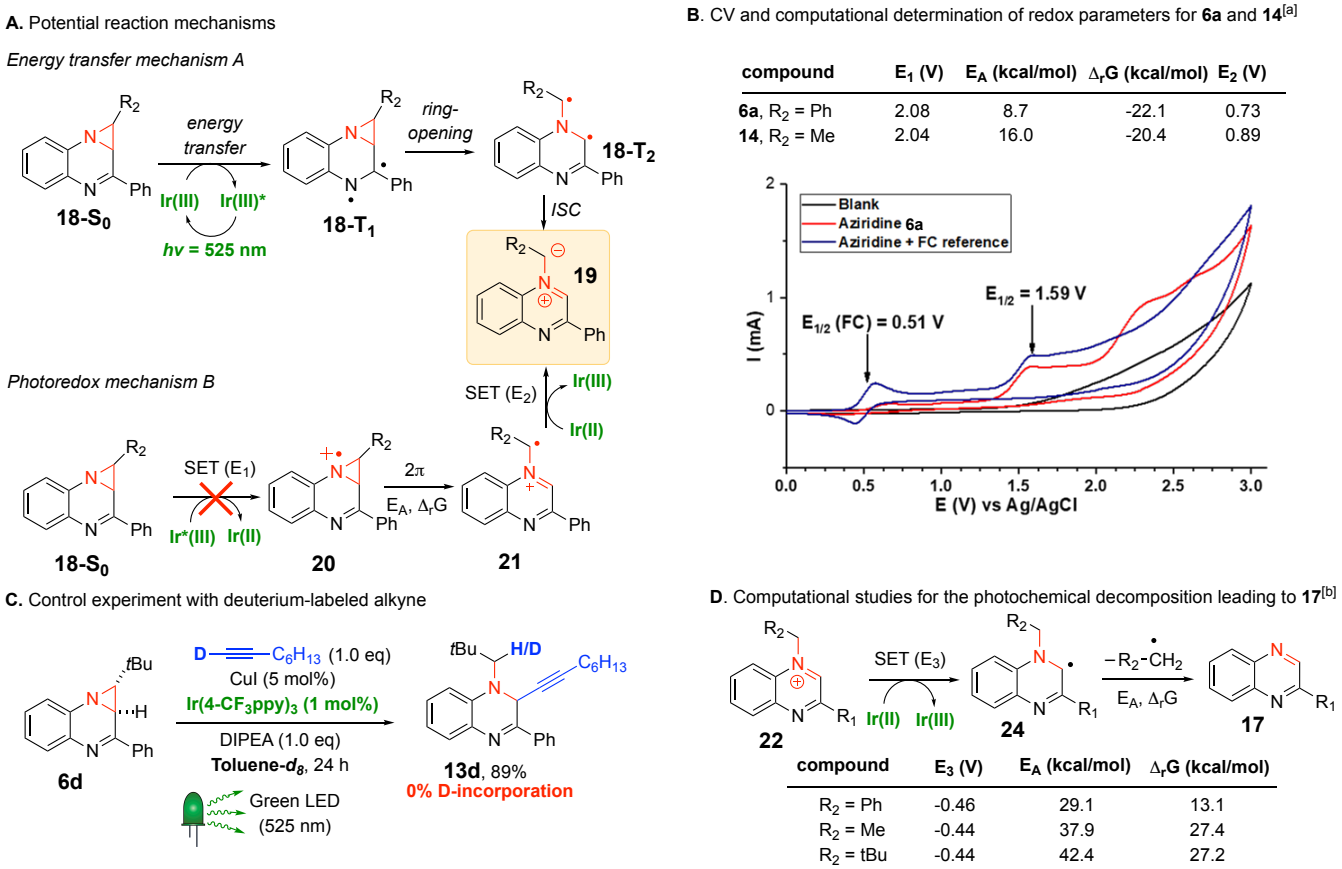

[a], [b] Calculations of redox potentials were performed using SMD(Toluene)/wB97x-D3/cc-pVTZ, transition state search and entropy analysis was performed using B3LYP/6-31+G**, electronic energy was reevaluated at SMD(Toluene)/wB97x-D3/cc-pVTZ level of theory.

hydroxyls (**13o–13r**) did not lead to the formation of side products of competitive addition to quinoxalinium cations demonstrating high catalytic differentiation of Cu(I) catalysis towards alkyne addition. Similarly, the reaction proceeded smoothly with propargyl acetate to provide product **13s** in 88% yield. The variation in the C_2-substituent of aziridinoquinoxalines was explored next (**13t-13z**). The introduction of both electron withdrawing (**13u-13x**) and electron donating (**13t**) substituents at the *para*-position of the C_2- phenyl ring did not impact the yield and the corresponding adducts were obtained in 82-96% yield. Similarly, the C_2-naphthyl-substituted product **13y** was formed in excellent 88% yield. At the same time, the 2-furanyl substituted product **13y** was isolated in only 36% yield due to significant decomposition presumably due to the side-reactions of furan under the photochemical conditions. In the case of C_2-thiophen substituted substrate **6z**, reaction proceeded without any signs of decomposition with 51% coversion by NMR resulting in 44% yield of **13z** and recovered starting material. Low conversion can be attributed to Ir(III) photocatalyst poisoning by the sulfur heterocycle. Finally, the substrates containing the cyclohexyl- and isopropyl-substituents at the aziridine ring, **6aa** and **6ab** were subjected to reaction with acetylene **12a** to provide products **13aa** and **13ab** in 67% and 50% yield, correspondingly.

After establishing the optimal conditions for green LED-induced alkyne addition to aziridinoquinoxalines, our subsequent studies focused on developing the asymmetric variant of this reaction (Table 3 and SI-II-3).[10,11] Various PyBox ligands (**L4-L9**) demonstrated low-to-moderate enantioselectivities (entries 1-6), while the best enantiomeric ratio (e.r.) of 82:18 was obtained using either tertbutyl (**L8**) or adamantly (**L9**) derivative of Py-Box (entries 5-8). Further reaction optimization by reducing the catalytic loading of ligand **L8** to 2.5 mol% (Cu/L = 2:1 ratio) helped to increase the e.r. to 87:13 for product **13a** (entry 8). Excellent enantioselectivity (95:5) can be obtained using (*S,R*)-*N*-PINAP ligand **L2**[12] (entries 9-10) albeit product **13a** was isolated in only 25% yield due to significant decomposition to 2-phenylquinoxaline **17**. As aziridinoquinoxaline **6d** previously exhibited higher stability then **6a**, we tested it with ligand **L2** in THF and the resultant isolated product **13d** was formed in 81% yield and 93:7 er. Further attempts to optimize the reaction conditions by evaluating copper(I) chloride, copper(I) or copper(II) trifluoromethanesulfonates as the catalysts did not lead to improved yields or selectivities (*cf.* Table SI-5). Therefore, the conditions for the formation of **13d** with PINAP ligand **L2** (entry 11) were selected for further evaluation (*cf.* Scheme 3). Using the optimized conditions with ligand **L2** for the formation of chiral **13a** and **13d**, we explored the scope of this transformation using *tert*-butyl-substituted aziridinoquinoxalines next (Scheme

3). Changing TMS-substituted alkyne **12a** to bulkier TES-protected alkyne **12b** resulted in more enantioselective formation of the product **13e** (94.5:5.5 e.r.). However, the use of phenylacetylene lowered both the selectivity and the yield for the formation of product **13h** (68% yield, 87.5:12:5 e.r.). The subsequent reactions with TES-substituted alkyne **12b** produced chiral substrates **13ac-13ag**. In general, introduction of an electron withdrawing substituent at the *para*-position of the C_2-phenyl ring resulted in similar e.r. values, but lower yield. Thus, *p*-CF_3-substituted substrate **6u** provided the corresponding product in 59% yield and 92.5:7.5 e.r., *p*-MeOCO-substituted substrate **6v** led to product **13ae** in 58% yield and 94.5:5.5 e.r., and the use of *p*-CN-substituted **6w** resulted in **13af** in 63% yield and 96:4 e.r. The configuration of 13af was determined via X-ray crystallographic analysis and was assigned as (*R*).[22] At the same time, substitution with *p*-methoxy, and *p*-fluoro groups resulted in enantioselectivity erosion, and products **13ac** and **13ag** were obtained in 57% yield, 87:13 e.r. and 67% yield, 90:10 e.r., correspondingly. With the aforementioned results in hands, our next studies were focused on getting further insights into the mechanism of these photochemical transformations. The entire transformation involves cooperative catalysis of Ir(III) and Cu(I) and consists of three stages i) photocatalysis with Ir(III) leading to formation of azomethine ylide; ii) formation of copper(I) acetylide; iii) reaction of copper(I) acetylide and azomethine ylide.

Our computational and fluorescence studies helped to shed some light onto the possible role of the initial stages of the photochemical cascade leading to the formation of azomethine ylide. Ir(III) photocatalysts usually are excited by Blue LEDs (400-440 nm) and we are not aware of using light with longer wavelengths such as Green LED (λ_{max}=525 nm) to promote either photoredox or energy transfer reactions with Ir(III). Recorded fluorescent spectrum of Ir(4-CF_3-ppy)$_3$ demonstrates typical wide absorption in 250-450 nm range that matches perfectly the spectrum of typical Blue LEDs; however, the absorption of Ir(III) and emission of Green LED spectra have minor overlap near 490-500 nm region (cf. Figure SI-9). The emission of the employed Green LED light source seems to be sufficient to perform EnT mechanism in studied reaction. The emission of the photocatalyst also perfectly matches the energy of the computed and measured triplet state (Scheme 3A-C). While the photoexcited Ir(III) catalyst may facilitate **18-T1** formation via energy transfer mechanism (Scheme 4A), another possibility to consider is the photoredox mechanism proceeding through radical cation intermediates **20** and **21**.[23] Mechanism A has already been investigated computationally (Table 1, Scheme 2A, and SI-IV-1,5); however, to gain better understanding of Mechanism B, DFT computations (TD-DFT, SMD/wB97x-D3/cc-pVTZ) were carried out (Scheme 4C and Table SI-IV-2,3). At first step, aziridinoquinoxaline **18-S$_0$** may undergo a SET oxidation to form cation radical **20**, for which the oxidation potential is estimated to be around E_1 = 2.0 V in toluene for both phenyl- and methyl-substituted aziridinoquinoxalines **6a** and **14**. In THF and acetonitrile this potential is lowered to 1.5 V and 1.3 V, respectively. The subsequent ring-opening of radical-cation **20** has low energy barrier for R_2 = Ph (8.7 kcal/mol) and slightly higher barrier for R_2 = Me (16.0 kcal/mol), but in both cases this step should be feasible. In addition, the ring-opening of radical-cation **20** is thermodynamically favored by approximately 20 kcal/mol (Gibbs free energy). Finally, the generation of ylide **21** should also proceed easily due to low reduction potential of open radical-cation **21** (E_2 = 0.7 to 0.9 V). For this alternative mechanism B, there are two key steps involving SET process, first is the oxidation of aziridinoquinoxalines, and second is the final reduction of the open form of radical-cation **21** to ylide **19**. The reduction of **21** to ylide **19** should be possible by any Ir(II) photocatalyst present in the reaction mixture as for Ir(III)/Ir(II) redox reaction potentials are in range of –1.3 to –2.2 V (Scheme SI-2). However, the first oxidation step of **18-S$_0$** may have a potential mismatch with the oxidation potential of the excited Ir(III) photocatalyst (highest potential E = 1.21 V, Scheme SI-2). To confirm this, a cyclic voltammetry study was performed on aziridinoquinoxaline **6a** in acetonitrile (Scheme 4B) demonstrating irreversible oxidation of **6a** with half wave at 1.49 V (vs SCE, corrected with ferrocene). The measured potential matches well computed 1.36 V in MeCN by the DFT studies. Based on this we can make a conclusion that the proposed SET mechanism B cannot be operational under current photochemical conditions since Ir(4-CF_3-ppy)$_3$ is not a sufficiently strong oxidant to generate radical-cation **20**.

To probe the last step of the mechanism involving the reaction of copper(I) acetylide and ylide, (*cf.* Schemes 1), the reaction of **6d** and D-labeled alkyne **12j** was investigated using the standard protocol (Scheme 4C). as the substrate was used to probe both the deprotonation step by DIPEA as well as the following H/D-transfer to ylide **10**. If this mechanistic hypothesis is correct, then we should observe D-incorporation in final product **13d**. While the reaction with D-labeled **12k** proceeded as usual, the resultant product **13d** was isolated in 89% yield with no deuterium incorporation. As the deuterated toluene (d8-toluene) was used in the reaction, only DIPEA may serve as the source of hydrogen atoms that is protonating the ylides instead of alkyne. This process may involve oxidation of the intermediate ylide **19** with Ir(III) to form intermediate **21** that subsequently undergoes HAT reaction with DIPEA to form protonated quinoxalinium ion that undergoes a reaction with copper(I) acetylide.

Finally, we were seeking to explain consistently observed decomposition of aziridinoquinoxaline to 2-phenylquinxaline **17** (Scheme 4D). The product-to-decomposition ratio depended on the solvent used as well as chiral ligand and copper(I) salt. This led us to the hypothesis that there is a competitive decomposition mechanism(s) to product formation and the reaction conditions may regulate the favoring pathway. We envisioned that the generated quinoxalinium intermediates **22** should have similar properties to *N*-alkylpyridinium (Katrizky's) salts,[24] which are well-known to undergo radical extrusion after the SET reduction. Similarly, the reduction of quinoxalinium ion intermediates **22** to radical-cation **23** followed by the radical extrusion will lead to 2-phenylquinoxaline **17**. Therefore, we calculated the reduction potential for intermediates **22** to radical **23** (Scheme 4D and Table SI-19). DFT calculations at ωB97X-D3/cc-pVTZ level of theory and SMD solvation model (for Toluene, Acetonitrile and THF) provided values ranging from –0.35 to –0.65 V (–0.45 V for toluene specifically). Therefore, the reduction of **22** can be accomplished with Ir(II) species generated by Ir(III) reduction with DIPEA. The subsequent step involving the C-N bond dissociation leading to **4** has high barriers (Scheme 4D), but phenyl-substituted aziridinoquinoxaline **6a** (R_2 = Ph) decomposition proceeds with lower activation energy (29.1 kcal/mol) in comparison to the methyl (37.9 kcal/mol) and t*ert*-butyl (42.4 kcal/mol) derivatives **14** and **6d**. Such difference in activation energy can be explained by the formation of a more stable benzyl

radical, and it is consistent with our prior observations of lower photochemical stability of phenyl-substituted substrates **13a-c** in comparison to **6d** and related compounds.

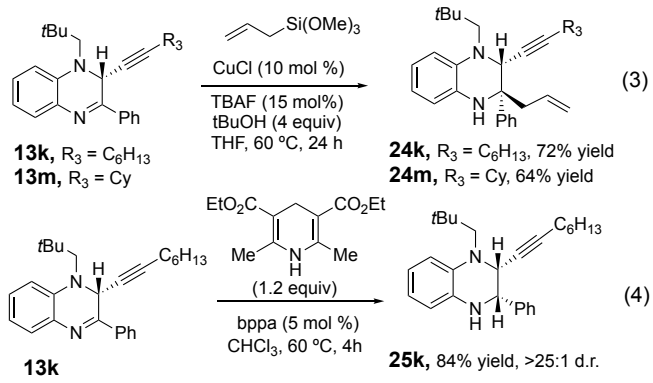

The dihydroquinoxaline products **13** contain multiple functional groups that may enable their functionalization into more complex quinoxaline derivatives (Eq. 3 and 4). Thus, the C=N moiety of substrates **13k** and **13m** may undergo Cu(I)-catalyzed allylation with allyltrimethoxysilane to provide **24k** and **24m** in 72% and 64% yield as anti-diastereomers only (Eq. 3).[25] Similarly, subjecting **13k** to the reaction with stoichiometric Hantzsch ester resulted in *syn*-diasteromer **25k** in 84% yield and >25:1 d.r. (Eq. 4). It is noteworthy that tetrahydroquinoxalines **24** and **25** cannot be easily derived by other methods such as hydrogenation of quinoxalines.

Conclusion

In summary, this manuscript describes a new method for accessing dihydroquinoxalines from readily available aziridinoquinoxalines. While aziridinoquinoxalines undergo C=N addition reaction with nucleophiles, we have discovered a photochemical method that enables alkyne addition to the aziridine, rather than imine, moiety of the aziridinoquinoxalines. While the attempts to accomplish this transformation using thermal activation or direct photolysis with Blue LED as the light source were not successful, the computational studies helped to discover a dual Ir(III)/Cu(I) catalytic system that promotes alkyne addition under green LED photolysis (λ_{max} = 525 nm). This mild method features high levels of chemo- and regioselectivity and was used to generate 29 highly functionalized substituted dihydroquinoxalines (**13a-13ab**) in 44-98% yield. This transformation was also carried asymmetrically using *(S,R)-N*-PINAP (**L2**) as the chiral ligand to provide 9 chiral addition products in 96:4 to 86:14 e.r. These dihydroquinoxaline products may serve as the substrates for further functionalization to provide highly functionalized tetrahydroquinoxalines that cannot be easily obtained using other methods. The experimental and theoretical explorations of this photochemical reaction suggest a mechanism that involves Ir(III)-catalyzed triplet energy transfer mechanism followed by a ring-opening reaction ultimately leading to the formation of azomethine ylide intermediates. These azomethine intermediates undergo sequential protonation to provide quinoxalinium ion intermediates that undergo copper(I) acetylide addition. To the best of our knowledge, this is the first example of successful generation and trapping of azomethine ylides with visible light under mild conditions, and further exploration of these transformation is the subject of the ongoing work in our laboratories.

ASSOCIATED CONTENT

Supporting Information

The authors have cited additional references within the Supporting Information.[7e, 19, 25-35]

Acknowledgements

P.N. thanks NIH R35GM136341 grant for supporting these studies. P.M.Z. thanks the NIH for support through R35GM128830. O.Z. thanks the University of Michigan Rackham Pre-Doctoral Fellowship. R. J. S. acknowledges the Center for Crystallographic Research and Support from the MRI program by the National Science Foundation under Grant No. 1919565 for the Purchase of the Rigaku Synergy S Diffractometer at MSU.

AUTHOR INFORMATION

Corresponding Author

* nagorny@umich.edu
* paulzim@umich.edu

REFERENCES

1) a) M. M. Heravi, V. Zadsirjan, *RSC Adv. Synth* **2020**, *10*, 44247; b) E. Vitaku, D. T. Smith, J. Njardarson, *J. Med. Chem.* **2014**, *57*, 10257; c) P. Bhutani, G. Joshi, N. Raja, N. Bachhav, P. K. Rajanna, H. Bhutani, P. A. Paul, R. Kumar, *J. Med. Chem.* **2021**, *64*, 2339.

2) a) A. C. Flick, C. A. Leverett, H. X. Ding, E. L. McInturff, S. J. Fink, S. Mahapatra, D. W. Carney, E. A. Lindsey, J. C. DeForest, S. P. France, S. Berritt, S. V. Bigi-Botterill, T. S. Gibson, R. B. Watson, Y. Liu, C. J. O'Donnell, *J. Med. Chem.* **2022**, *65*, 9607; b) A. C. Flick, C. A. Leverett, H. X. Ding, E. L. McInturff, S. J. Fink, S. Mahapatra, D. W. Carney, E. A. Lindsey, J. C. DeForest, S. P. France, S.Berritt, S. V. Bigi-Botterill, T. S. Gibson, Y. Liu, C. J. O'Donnell, *J. Med. Chem.* **2021**, *64*, 3607.

3) a) M. G. Vinogradov, O. V. Turova, S. G. Zlotin, *Org. Biomol. Chem*. **2019**, *17*, 3670; b) Y.-C. Zhang, F. Jiang, F. Shi, *Acc. Chem. Res*. **2020**, *53*, 425; c) J. Yu, D.-F. Chen, L.-Z. Gong, *Pure Appl. Chem*. **2014**, *86*, 1217; d) P. A. Magriotis, *RSC Med. Chem*. **2020**, *11*, 745.

4) a) K. Torisu, K. Kobayashi, M. Iwahashi, Y Nakai, T. Onoda, T. Nagase, I. Sukimoto, Y. Okada, R. Matsumoto, F. Nanbu, S. Ohuchida, H. Nakai, M. Toda, *Bioorg. Med. Chem.* **2004**, *12*, 5361; b) J. E. Wilson, R. Kurukulasuriya, M. Reibarkh, M. Reiter, A. Zwicker, K. Zhao, F. Zhang, R. Anand, V. J. Colandrea, A.-M. Cumiskey, A. Crespo, R. A. Duffy, B. A. Murphy, K. Mitra, D. G. Johns, J. L. Duffy, P. Vachal *ACS Med. Chem. Lett*. **2016**, *7*, 261; c) R. P. Law, S. J. Atkinson, P. Bamborough, C. Chung, E. H. Demont, L. J. Gordon, M. Lindon, R. K. Prinjha, A. J. B. Watson, D. J. Hirst, *J. Med. Chem*. **2018**, *61*, 4317.

5) Selected examples: a) M. Rueping, F. Tato, F. R. Schoepke *Chem. Eur. J*. **2010**, *16*, 2688; b) Z.; Zhang, H. Du, *Angew. Chem. Int. Ed.* **2014**, *54*, 623; *Angew. Chem.* **2014**, *127*, 633; c) S. Li, W. Meng, H. Du, *Org. Lett.* **2017**, *19*, 2604.

6) a) J. Huang, G. Li, G. Yang, D. Fu, X. Nie, X. Cui, J. Zhao, Z. Tang, *Chem. Sci.* **2021**, *12*, 4789; b) Z. Luo, Z. Li, H. Zhao, J. Yang, L. Xu, M. Lei, Q. Fan, P. J. Walsh, P. J. *Angew. Chem. Int. Ed.* **2023**, *8*, e202305449; c) C. Liu, X. Liu, Q. Liu, *Chem* **2023**, *9*, 2585.

7) a) Z. Sun, G. A. Winschel, A. Borovika, P. Nagorny, *J. Am. Chem. Soc.* **2012**, *134*, 8074; b) Z. Sun, G. A. Winschel, P. M. Zimmerman, P. Nagorny, *Agew. Chem. Int. Ed.* **2014**, *53,* 11194; c) S. Sun, P. Nagorny,

Chem. Commun. **2020**, *56*, 8432; d) O. Zhelavskyi, Y.-J. Jhang, P. Nagorny, *Synthesis* **2023**, *55*, 2361; e) Y.-J. Jhang, O. Zhelavskyi, P. Nagorny, *Org. Lett.* **2023**, *25*, 7721.

8) a) H. W. Heine, R. P. Henzel, *J. Org. Chem.* **1969**, *34*, 171; b) A. I. Zbruyev, V. V. Vashchenko, A. A. Andryushchenko, S. M. Desenko, V. I. Musatov, I. V. Knyazeva, V. A. Chebanov, *Tetrahedron* **2007**, *63*, 4297; c) V. D. Orlov, N. P. Vorob'eva, A. A. Tishchenko, O. M. Pikalev, V. I. Popov, L. M. Yaupol'skii, *Chem. Heterocycl. Comp.* **1991**, *27*, 942; d) V. A. Chebanov, A. I. Zbruyev, S. M. Desenko, V. D. Orlov, F. G. Yaremenko, *Curr. Org. Chem.* **2008**, *12*, 792; e) V. M. Muzalevskiy, A. Y. Rulev, E. V. Kondrashov, A. R. Romanov, I. A. Ushakov V. A. Chertkov, V. G. Nanajdenko, *Eur. J. Org. Chem*. **2016**, *8*, 11612.

9) Recent reviews: a) B. V. Rokade, J. Barker, P. J. Guiry, *Chem. Soc. Rev.* **2019**, *48*, 4766; b) S. Shah, B. G. Das, V. K. Singh, *Tetrahedron* **2021**, *93*, 132238; c) J. Farhi, I. N. Lykakis, G. E. Kostakis, *Catalysis* **2022**, *12*, 660.

10) Selected examples of asymmetric addition of copper(I) acetylides to imines: a) N. Gommermann, C. Koradin, P. Kurt, P. Knochel, *Angew. Chem. Int. Ed.* **2003**, *42*, 5763; *Angew. Chem.* **2003**, *115*, 5941; b) H. Dube, N. Gommermann, P. Knochel, *Synthesis* **2004**, *12*, 2015; c) N. Gommermann, P. Knochel, *Chem.-Eur. J.* **2006**, *12*, 4380; d) Knopfel, T. F.; P. Aschwanden, T. Ichikawa, T. Watanabe, E. M. Carreira, *Angew. Chem. Int. Ed.* **2004**, *43*, 5971; *Angew. Chem*. **2004**, 116, 6097; e) P. Aschwanden, C. R. J. Stephenson, E. M. Carreira, *Org. Lett.* **2006**, *8*, 2437; f) F. S. P. Cardoso, K. A. Abboud, A. Aponick, *J. Am. Chem. Soc.* **2013**, *135,* 14548; g) P. H. S. Paioti, K. A. Abboud, A. Aponick, *J. Am. Chem. Soc*. **2016**, *138*, 2150; h) P. H. S. Paioti, K. A. Abboud, A. Aponick, *ACS Catalysis* **2017**, *7*, 2133; i) H. Naeimi, M. Moradian, *Tetrahedron: Asymmetry* **2014**, *25*, 429; j) C. Zhao, D. Seidel, *J. Am. Chem. Soc*. **2015**, *137*, 4650; k) B. V. Rokade, P. J. Guiry, *ACS Catalysis* **2017**, *7*, 2334; l) B. V. Rokade, P. J. Guiry, *J. Org. Chem*. **2019**, *84*, 5763; m) Q. Liu, H. Xu, Y. Li, Y. Yao, X. Zhang, Y. Guo, S. Ma, *Nature Commun*. **2021**, *12*,1.

11) Selected examples of enantioselective copper(I) acetylide addition to generate chiral nitrogen-containing heterocycles: a) Z. Li, C.-J. Li, *Org. Lett.* **2004**, *6*, 4997; b) A. M. Taylor, S. L. Schreiber, *Org. Lett*. **2006**, *8*, 143; c) Z. Sun, S. Yu, Z. Ding, D. Ma, *J. Am. Chem. Soc*. **2007**, *129*, 9300; d) D. A. Black, R. E. Beveridge, B. A. Arndtsen, *J. Org. Chem*. **2008**, *73*, 1906; e) T. Hashimoto, M. Omote, K. Maruoka, *Angew. Chem. Int. Ed.* **2011**, *50*, 8952; f) W. Lin, T. Cao, W. Fan, Y. Han, J. Kuang, H. Luo, B. Miao, X. Tang, Q. Yu, W. Yuan, J. Zhang, C. Zhu, S. Ma, *Angew. Chem. Int. Ed*. **2014**, *53*, 277; g) W. Lin, S. Ma, *Org. Chem. Front.*, **2014**, *1*, 338; h) S. Sun, C. Li, P. E. Floreancig, H. Lou, L. Liu, *Org. Lett*. **2015**, *17*, 1684; i) W. Lin, S. Ma, *Org. Chem. Front.*, **2017**, *4*, 958; j) S. Zhou, R. Tong, *Org. Lett.* **2017**, *19*, 1594; k) J. Yu, Z. Zhang, S. Zhou, W. Zhang, R. Tong, *Org. Chem. Front.,* **2018**, *5*, 242; l) P.-S. Gao, X.-J. Weng, Z.-H. Wang, C. Zheng, B. Sun, Z.-H. Chen, S.-L. You, T.-S. Mei, *Angew. Chem. Int. Ed*. **2020**, *59*, 15254; m) W. Guan, S. O. Santana, J. Liao, K. Henninger, M. P. Watson, *ACS Catal*. **2020**, *10*, 13820; n) L. Liang, S. Zhou, W. Zhang, R. Tong, *Angew. Chem. Int. Ed.* **2021**, *60*, 25135; o) D. M. Morgan, C. M. Reid, P. J. Guiry, *J. Org. Chem.* **2023**, *ASAP*, DOI: 10.1021/acs.joc.3c01944.

12) a) P. Zarotti, T. F. Knopfel, P. Aschwanden, E. M. Carreira, *ACS Catal*. **2012**, *2*, 1232; b) S.-J. Han, V. Bhat, B. M. Stoltz, S. C. Virgil, *Adv. Synth. & Catal*. **2019**, *361*, 441.

13) a) H. W. Heine, R. Peavy, *Tetrahedron Lett*. **1965**, *35*, 3123; b) A. Padwa, L. Hamilton, *Tetrahedron Lett.* **1965**, *6*, 4363; c) R. Huisgen, W. Scheer, G. Szeimies, H. Huber, *Tetrahedron Lett.* **1966**, *4*, 397; d) R. Huisgen, W. Scheer, H. Huber, *J. Am. Chem. Soc*. **1967**, *89*, 1753; e) R. Huisgen, W. Scheer, *Tetrahedron Lett.* **1971**, *6*, 481.

14) H. Bouas-Laurent, H. Durr, *Pure Appl. Chem*. **2001**, *73*, 639.

15) A. F. Khlebnikov, M. S. Novikov, *Chem. Het. Comp*. **2012**, *48*, 179.

16) a) A. I. Zbruev, O. V. Shishkin, A. O. Doroshenko, S. M. Desenko, V. A. Chebanov, *J. Photochem. & Photobiol. A: Chemistry* **2018**, *353*, 469.

17) For the overview of aziridine reactions with alkynes and related nucleophiles refer to: a) X. E. Hu, *Tetrahedron* **2004**, *60*, 2701; b) J.-J. Feng, J. Zhang, *ACS Catal*. **2016**, *6*, 6651; c) S. Sabir, G. Kumar, V. P. Verma, J. L. Jat, *ChemistrySelect* **2018**, *3*, 3702; d) Z. Chai, *Synthesis* **2020**, *52*, 1738.

18) C. Zhang, D. Seidel, *J. Am. Chem. Soc.* **2010**, *132*, 1798.

19) a) P. M. Zimmerman, *J. Chem. Phys.* **2013**, *138*, 184102; b) P. M. Zimmerman, *J. Comput. Chem.* **2013**, *34*, 1385; c) P. M. Zimmerman, *J. Comput. Chem.* **2015**, *36*, 601; d) P. M. Zimmerman, *J. Chem. Theory Comput.* **2013**, *9*, 3043.

20) a) F. Strieth-Kalthoff, M. J. James, M. Teders, L. Pitzer, F. Glorius, *Chem. Soc. Rev.* **2018**, *47*, 7190; b) C. K. Prier, D. A. Rankic, D. W. C. MacMillan, *Chem. Rev*. **2013**, *113*, 5322.

21) For examples of UV-spectral data of azomethine ylides refer to: a) R. Huisgen, K. Niklas, *Heterocycles* **1984**, *22*, 21; b) E. Vedejs, S. Dax, G. R. Martinez, C. K. McClure, *J. Org. Chem*. **1987**, *52*, 3471.

22) Deposition number 2312298 (for **13af**), contains the supplementary crystallographic data for this paper. These data are provided free of charge by the joint Cambridge Crystallographic Data Centre and Fachinformationszentrum Karlsruhe Access Structures service.

23) For examples of aziridine transformations involving redox mechanisms refer to: a) H. Sun, C. Yang, R. Lin, W. Xia, *Adv. Synth. Catal.* **2014**, *356*, 2775; b) W. Hao, X. Wu, J. Z. Sun, J. C. Siu, S. N. MacMillan, S. Lin, *J. Am. Chem. Soc*. **2017**, *139*, 12141; c) Y. Li, F. Chen, S. Zhu, L. Chu, *Org. Chem. Front.* **2021***, 8*, 2196; d) C. Yao, A. D. N. Williams, Y. Gu, J. R. Norton, *J. Org. Chem.* **2022**, *87*, 4991; e) W. L. Williams, N. E. Gutierrez-Valencia, A. G. Doyle*, J. Am. Chem. Soc.* **2023**, *145*, 24175.

24) Y. Gao, S. Jiang, N.-D. Mao, H. Xiang, J.-L. Duan, X.-Y. Ye, L.-W. Wang, Y. Ye, T. Xie, *Top. Curr. Chem*. **2022**, *380*, 1.

25) S. Yamasaki, K. Fujii, R. Wada, M. Kanai, M. Shibasaki, *J. Am. Chem. Soc.* **2002**, *124*, 6536.

26) J. Comelles, A. Pericas, M. Moreno-Mañas, A. Vallribera, G. Drudis-Solé, A. Lledos, T. Parella, A. Roglans, S. García-Granda, L. Roces-Fernández, *J. Org. Chem.* **2007**, *72*, 2077.

27) A. Paul, R. Borrelli, H. Bouyanfif, S. Gottis, F. Sauvage, *ACS Omega* **2019**, *4*, 14780.

28) B. Hwang, M. S. Park, K. Kim, *ChemSusChem* **2015**, *8*, 310.

29) C. M. Cardona, W. Li, A. E. Kaifer, D. Stockdale, G. C. Bazan, *Adv. Mater.* **2011**, *23*, 2367.

30) Y. Shao, Z. Gan, E. Epifanovsky, A. T. B. Gilbert, M. Wormit, J. Kussmann, A. W. Lange, A. Behn, J. Deng, X. Feng, X., et al. *Mol. Phys.* **2015**, *113*, 184.

31) W. Humphrey, A. Dalke, K. Schulten, *J. Mol. Graph.* **1996**, *14*, 33.

32) A. D. Becke, *J. Chem. Phys.* **1993**, *98*, 5648.

33) W. J. Hehre, R. Ditchfield, J. A. Pople, F. T. Wall, L. A. Hiller, D. J. Wheeler, J. Chern Phys, J. M. Hammersley, K. W. Morton, J. Roy Stat Soc, et al. *J. Chem. Phys.* **1972**, *56*, 2257.

34) Y. S. Lin, G. De Li, S. P. Mao, J. Da Chai, *J. Chem. Theory Comput.* **2013**, *9*, 263.

35) R. A. Kendall, T. H. Dunning, R. J. Harrison, *J. Chem. Phys.* **1992**, *96*, 6796.

36) S. Hirata, M. Head-Gordon, *Chem. Phys. Lett.* **1999**, *314*, 291.